

# Impact of Dimethylformamide, Tetrahydrofuran, and Dimethyl Sulfoxide on Bulk Heterojunction Organic Solar Cells' Efficiency and Environmental Footprint

Fernando Rodríguez-Mas,\* David Valiente, Pablo Corral, José Luis Alonso, and Susana Fernández de Ávila

Organic solar cells (OSCs), especially those employing bulk heterojunction architecture, present a promising avenue in renewable energy technology. These devices utilize organic materials and can be doped by solvents such as dimethylformamide (DMF), tetrahydrofuran (THF), and dimethyl sulfoxide (DMSO). Solvent doping (DMF, THF, and DMSO) is observed to augment the efficiency of OSCs. However, a trade-off exists between the volume of solvent used and the device's efficiency. The judicious selection of solvents is crucial as it directly impacts the environmental footprint of the fabrication process and the power conversion efficiency. Notably, the use of solvents in OSC fabrication contributes to reducing the environmental impact across various categories, in particular Abiotic Depletion, Global Warming, and Human Toxicity. Among the solvents studied, THF demonstrates the most significant reduction in environmental impact. Therefore, optimizing the choice and volume of solvents in OSC fabrication is paramount for achieving both enhanced device performance and minimal environmental footprint.

## 1. Introduction

Despite the growing transition toward the utilization of renewable energy sources in contemporary society, the electricity generation matrix remains predominantly reliant on the utilization of fossil fuels,<sup>[1]</sup> as depicted in **Figure 1**. While a gradual shift toward more sustainable and clean sources,<sup>[2]</sup> such as solar

and wind energy,<sup>[3]</sup> is evident, the persistent dependence on fossil fuels suggests that society's energy consumption could be linked to the combustion of these non-renewable resources. This phenomenon underscores the imperative need for a more accelerated transition toward sustainable energy practices, considering the environmental impact and the significance of mitigating the consumption of nonrenewable energy sources.

Photovoltaic cells offer a series of significant advantages compared to fossil fuels as an energy solution. First, they directly generate electricity from solar radiation,<sup>[4]</sup> rendering it a renewable energy source.<sup>[5]</sup> This feature drastically reduces emissions of greenhouse gases and other pollutants associated with fossil fuel combustion,<sup>[6]</sup> thereby contributing to mitigate climate change<sup>[7]</sup> and improving air quality.<sup>[8]</sup>


Photovoltaic cells are capable of generating electricity in a decentralized way,<sup>[9]</sup> meaning they can be installed in a wide variety of locations, from building rooftops<sup>[10]</sup> to remote or rural areas lacking access to the electrical grid.<sup>[11]</sup> This reduces dependence on centralized and vulnerable infrastructures, such as fossil-fuel-powered plants, and enhances the resilience and energy security of communities by diversifying available energy sources.<sup>[11]</sup> All in all, photovoltaic cells represent a sustainable and versatile alternative to fossil fuels,<sup>[12]</sup> offering significant environmental,<sup>[13]</sup> economic,<sup>[14]</sup> and social benefits<sup>[15]</sup> on a global scale.

The development and implementation of photovoltaic panels are intrinsically linked to the sustainable development goals (SDGs) of the 2030 Agenda of the United Nations.<sup>[16]</sup> The expansion of solar energy through photovoltaic panels directly contributes to SDG 7 of the 2030 Agenda, which aims to ensure access to affordable, reliable, sustainable, and modern energy. By harnessing solar light, a renewable and inexhaustible energy source, photovoltaic panels help diversify the energy matrix, reduce reliance on fossil fuels, and facilitate access to electricity in remote or underserved areas.<sup>[17]</sup>

Furthermore, the deployment of solar panels supports SDG 13 of the 2030 Agenda, which seeks to take urgent action to combat climate change and its impacts.<sup>[18]</sup> By reducing greenhouse gas emissions and mitigating dependence on fossil fuels, photovoltaic panels contribute to climate change reduction while fostering

F. Rodríguez-Mas, D. Valiente, P. Corral, J. L. Alonso, S. Fernández de Ávila  
Communication Engineering Department  
Miguel Hernández University  
03202 Elche, Spain  
E-mail: fernando.rodriguezmas@umh.es

D. Valiente, J. L. Alonso, S. Fernández de Ávila  
University Institute for Engineering Research of Elche – I3E  
Miguel Hernández University  
03202 Elche, Spain

 The ORCID identification number(s) for the author(s) of this article can be found under <https://doi.org/10.1002/aesr.202400193>.

© 2024 The Author(s). Advanced Energy and Sustainability Research published by Wiley-VCH GmbH. This is an open access article under the terms of the Creative Commons Attribution License, which permits use, distribution and reproduction in any medium, provided the original work is properly cited.

DOI: 10.1002/aesr.202400193

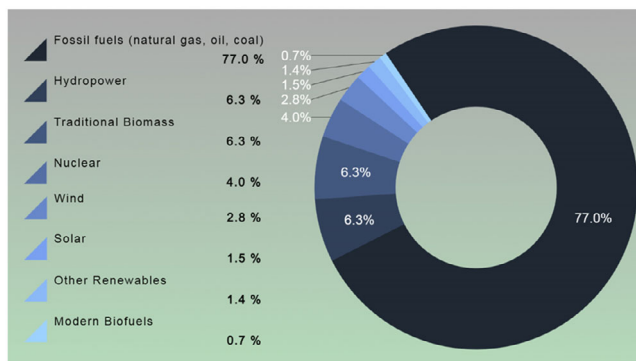


**Figure 1.** The global distribution of primary energy consumption across various sources in 2021. The data has been compiled from ref. [1].

the transition toward a low-carbon<sup>[18]</sup> and climate-resilient economy.<sup>[19]</sup>

The development of photovoltaic panels can also support SDG 9 of the 2030 Agenda, “Industry, Innovation, and Infrastructure”.<sup>[20]</sup> Research and innovation in solar technologies, including more efficient and affordable photovoltaic panels, are crucial to expand access to solar energy and accelerate the transition toward more sustainable and equitable energy systems. Collectively, the development of photovoltaic panels significantly contributes to achieving multiple goals of the 2030 Agenda, addressing key global challenges related to energy, climate, and sustainable development.

Currently, the photovoltaic industry is based on silicon technology.<sup>[21]</sup> Silicon production for photovoltaic installations faces several significant challenges impacting environmental sustainability.<sup>[22]</sup> The process of obtaining pure silicon is energy intensive and requires a considerable amount of resources, including electricity<sup>[23]</sup> and raw materials.<sup>[24]</sup> In addition, the availability of high-purity silicon can be a limiting factor in the expansion of large-scale solar energy. As the demand for photovoltaic panels increases, especially in the context of transitioning to a low-carbon economy, a shortage of quality silicon suitable for solar cell manufacturing could arise. This situation could trigger an increase in silicon prices, negatively impacting the profitability of photovoltaic installations and their competitiveness against other energy sources.

As an alternative, organic solar cells (OSCs) offer a promising solution to this issue. OSCs emerge as a crucial measure to address the energy and environmental challenge derived from the silicon purification, as discussed in ref. [25]. Within OSCs, devices based on bulk heterojunction (BHJ) stand out.<sup>[26–28]</sup> A BHJ-based OSC is a device that converts light energy into electricity through a photophysical process. In a BHJ OSC, a heterojunction interface is created by blending a donor (hole-transporting) polymer and an acceptor (electron-transporting) polymer. This configuration promotes the efficient separation of photoinduced excitonic pairs, essential for generating electric current.<sup>[29]</sup>

When the light impacts the device, photons generate electron-hole pairs. The released electrons are transported through the acceptor material to the electron-transport layer (ETL), while the holes migrate through the donor material to the

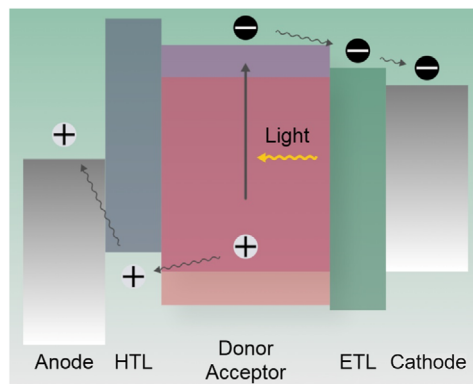


**Figure 2.** Functionality and carrier transport in an organic solar cell based on bulk heterojunction.

hole-transport layer (HTL). After migrating through the anode and cathode respectively, an electric current is generated in the external circuit, **Figure 2**. The efficiency of this charge transfer depends on the architecture and morphology of the BHJ structure, as well as the characteristics of the organic materials used.

Among the possibilities of OSCs studied by the scientific community,<sup>[30–32]</sup> one extensively investigated is formed by the following structure: indium tin oxide (ITO)/poly(3,4-ethylenedioxythiophene):poly(styrene sulfonate) (PEDOT:PSS)/poly(3-hexylthiophene): [6,6]-phenyl-C61-butyric acid methyl ester (P3HT:PCBM)/aluminum (Al).

This architecture constitutes a BHJ device, where the PEDOT:PSS polymer blend acts as an HTL, the P3HT:PCBM blend serves as the donor-acceptor material, and the aluminum functions as the cathode.

The blend of P3HT and PCBM polymers is prepared in a [1:0.8] weight ratio. The layer formed between these two polymers is also known as the active layer. PCBM belongs to the fullerene family and is recognized as an organic n-type semiconductor.<sup>[33]</sup> P3HT is a thiophene with a chain of six carbon atoms linked in single bonds at the third position. This configuration characterizes it as an organic p-type semiconductor.<sup>[34]</sup> The combination of both polymers forms the basis of the BHJ configuration, where one acts as the donor material and the other as the acceptor material.<sup>[35]</sup> In contrast, PEDOT:PSS is employed to form the HTL. Similar to the case of P3HT:PCBM, PEDOT:PSS is also composed of two distinct polymers.<sup>[36]</sup> In this blend, PEDOT donates charges that are captured by PSS.<sup>[37]</sup>

Various research efforts have resulted in specific enhancements to the PEDOT:PSS layer of devices under a BHJ structure. One investigation was focused on annealing PEDOT:PSS films, adjusting temperatures within a range from 120 to 400 °C, thereby altering the properties of the PEDOT:PSS layer.<sup>[38]</sup> Other research endeavors have focused on doping the PEDOT:PSS layer with different materials. For instance, Reddy et al.<sup>[39]</sup> doped PEDOT:PSS with cadmium sulfide nanoparticles. Consequently, the spectral response of the device extended from ultraviolet-visible to the near-infrared region. Not only has doping with nanocrystals been done, but there are also different studies where the HTL has been doped with

organic solvents. The PEDOT:PSS layer doped with methanol increased its conductivity compared to a pristine layer.<sup>[40]</sup>

The use of organic solvents to enhance the conductivity of the HTL is highly intriguing, as in addition to the described improvements, there is also a wide range of solvents that can be analyzed to determine which would offer the most suitable performance for its operation. This research is focused on studying the effects on the electrical properties of OSCs, where the HTL was composed of PEDOT:PSS and doped with three different organic solvents (dimethylformamide [DMF], tetrahydrofuran [THF], and dimethyl sulfoxide [DMSO]). Furthermore, the environmental impact of their use in manufacturing was assessed and compared with devices without these solvents.

## 2. Experimental Section

### 2.1. Materials

For the manufacture of the OSCs, the following materials were employed: isopropyl alcohol, 1,2,4-trichlorobenzene, chlorobenzene, PCBM, acetone, DMF, PEDOT:PSS in a 1.3% water solution, P3HT, THF, and DMSO. These materials were used without further purification and were acquired from Sigma-Aldrich.

### 2.2. Characterization

To conduct the electrical characterization of OSCs, current density versus voltage ( $J-V$ ) curves were generated. This was accomplished by employing a Keithley 2400 Sourcemeter device along with a Newport Solar Simulator configuration. The Newport Solar Simulator included a xenon arc lamp and an AM1.5G filter. Measurements were performed under standard conditions.

### 2.3. OSC: Fabrication Method

The fabrication of OSCs was based on the spin-coating technique.<sup>[41,42]</sup> This method involves the successive deposition of thin films of semiconductor polymers dissolved in a solution onto a substrate, in this case, ITO-covered glass. Once the semiconductor polymer was deposited, solvent removal from the solution occurred through substrate rotation and heating processes, resulting in the formation of the film. The devices used in this research were fabricated on a glass coated with ITO. A layer of PEDOT:PSS was deposited on the ITO layer, followed by a layer of P3HT:PCBM on top of it. The PEDOT:PSS layer was deposited at 6000 rpm, and the P3HT:PCBM layer was deposited at 300 rpm. Following the completion of these procedures, metallization was executed via aluminum evaporation within a high-vacuum environment.

This research focused on the effect of incorporating different solvents into the PEDOT:PSS layer and its impact on OSCs. To investigate its effect, three series of devices were fabricated, each designated for a specific solvent: DMF, THF, and DMSO. Each series consisted of five different devices. Additionally, an OSC served as a reference in which the PEDOT:PSS layer was no solvent. In the remaining five devices of each series, the solvent was gradually included. **Table 1** describes the volume of DMF solvent

**Table 1.** Volume of PEDOT:PSS and DMF solvent used in the fabrication of each device.

OSCs	PEDOT:PSS/DMF	PEDOT:PSS	DMF
	Volume ratio	[ $\mu$ L]	[ $\mu$ L]
Reference	[1:0.0]	200	0
OSC_1.1	[1:1.0]	100	100
OSC_1.2	[1:1.5]	80	120
OSC_1.3	[1:2.0]	67	133
OSC_1.4	[1:2.5]	57	143
OSC_1.5	[1:3.0]	50	150

**Table 2.** Volume of PEDOT:PSS and THF solvent used in the fabrication of each device.

OSCs	PEDOT:PSS/THF	PEDOT:PSS	THF
	Volume ratio	[ $\mu$ L]	[ $\mu$ L]
Reference	[1:0.0]	200	0
OSC_2.1	[1:0.5]	133	67
OSC_2.2	[1:1.0]	100	100
OSC_2.3	[1:1.5]	80	120
OSC_2.4	[1:2.0]	67	133
OSC_2.5	[1:2.5]	57	143

**Table 3.** Volume of PEDOT:PSS and DMSO solvent used in the fabrication of each device.

OSCs	PEDOT:PSS/THF	PEDOT:PSS	THF
	Volume ratio	[ $\mu$ L]	[ $\mu$ L]
Reference	[1:0.0]	200	0
OSC_3.1	[1:1.0]	100	100
OSC_3.2	[1:2.0]	67	133
OSC_3.3	[1:3.0]	50	150
OSC_3.4	[1:4.0]	40	160
OSC_3.5	[1:5.0]	33	167

relative to the volume of PEDOT:PSS used for the fabrication of the OSCs, while **Table 2** details those doped with THF, and **Table 3** details those doped with DMSO. Furthermore, all tables provide information on the devices without solvent.

## 3. Results

### 3.1. OSC: Electrical Characterization

Characteristic curves for the OSCs were measured under standard conditions. These curves depict the electric current density generated under 1 sun illumination. From these curves, electrical

parameters characterizing the device can be calculated. The maximum short-circuit current density ( $J_{SC}$ ) is generated when the voltage is zero, and the maximum open-circuit voltage ( $V_{OC}$ ) occurs when the current density is zero. The power conversion efficiency (PCE) of OSCs is determined from the  $J$ - $V$  curve and represents the possibility of the device to convert incident light power into electric power. It is calculated as the ratio of the electrical power output of the device to the incident optical power, Equation (1). In contrast, the fill factor (FF) describes the uniformity of charge distribution within the device, Equation (2). A high FF indicates high efficiency in charge collection and good quality of contacts in the device

$$PCE = \frac{P_{MAX}}{P_{INC}} = \frac{J_{MPP} \cdot V_{MPP}}{P_{INC}} \quad (1)$$

$$FF = \frac{P_{MAX}}{J_{SC} \cdot V_{OC}} = \frac{J_{MPP} \cdot V_{MPP}}{J_{SC} \cdot V_{OC}} \quad (2)$$

where  $P_{MAX}$  is the maximum power generated by the OSC,  $J_{MPP}$  and  $V_{MPP}$  are the current density and voltage at the maximum power point, respectively, and  $P_{INC}$  is the incident power.

The electrical characteristics of the OSCs doped with different volumes of DMF in the PEDOT:PSS layer are illustrated in the **Figure 3** and **Table 4**. The PCE reaches its maximum in the OSC\_1.2 with a value of 1.53% and reaches its minimum in the OSC\_1.5. Additionally, when the PEDOT:PSS layer is formed with a volume ratio of [1:3.0] (OSC\_1.5), it obtains a lower efficiency value than the reference PCE. That is to say that the effect of using the solvent is no longer effective. This may be due to the device fabrication model. The fact that increasing the volume of solvent directly implies a reduction in the use of PEDOT:PSS, diminishing the effect of the polymer blend in the HTL. Regarding the maximum power ( $P_{MAX}$ ), the same trends as those mentioned for the PCE are observed, reaching its maximum in OSC\_1.2 and the minimum in OSC\_1.5.

For OSCs doped with THF (**Figure 4**, **Table 5**), it is observed that the  $V_{OC}$  remains more or less constant, while the  $J_{SC}$ ,  $P_{MAX}$ , and efficiency tend to increase. The PCE reaches its maximum in

**Table 4.** Electrical characteristics of the OSCs doped with DMF and OSC without solvent (reference).

OSCs	Reference	OSC_1.1	OSC_1.2	OSC_1.3	OSC_1.4	OSC_1.5
$V_{OC}$ [V]	0.58	0.53	0.53	0.52	0.51	0.50
$J_{SC}$ [ $\text{mA cm}^{-2}$ ]	4.13	4.73	6.82	6.43	6.32	4.70
$P_{MAX}$ [ $\text{mW cm}^{-2}$ ]	1.12	1.27	1.53	1.36	1.20	0.90
FF [%]	47	51	42	41	37	38
PCE [%]	1.11	1.27	1.53	1.36	1.20	0.90

the OSC\_2.3 device with a value of 1.66%, showing all devices in the series higher values than the reference.

To complete the electrical characterization of the OSCs, measurements of the  $J$ - $V$  curves were conducted on a series of OSCs doped with DMSO. Furthermore, these results were compared with those of the OSC utilizing the PEDOT:PSS layer without solvent, **Table 6** and **Figure 5**.

In this study, the maximum PCE was observed in OSC\_3.2. In this OSC, the HTL consists of one part by volume of PEDOT:PSS and two parts by volume of DMSO. For larger volumes of DMSO, the efficiency decreases; furthermore, the PCE is lower than that generated by the reference.

A similar behavior is observed for the three solvent series studied in this work. The use of polar solvents leads to an improvement in the efficiency of devices fabricated with selected doping conditions. Specifically, OSC\_1.2 achieves a value of 1.53%, OSC\_2.3 achieves a value of 1.66%, and OSC\_3.2 achieves a value of 1.27%. All of these values surpass the 1.1% efficiency of the reference OSC. However, after reaching the maximum, the PCE begins to decrease, and the relationship with the increase in solvent employed is lost. Studies have indicated that the increase in efficiency of solvent-doped devices may occur due to the presence of polar solvents, which decrease the intermolecular distance between PEDOT and PSS. This reduction in intermolecular distance generates an enhanced conductivity in the HTL. The presence of polar solvents reduces repulsions arising from Coulomb interactions within the PEDOT:PSS polymer

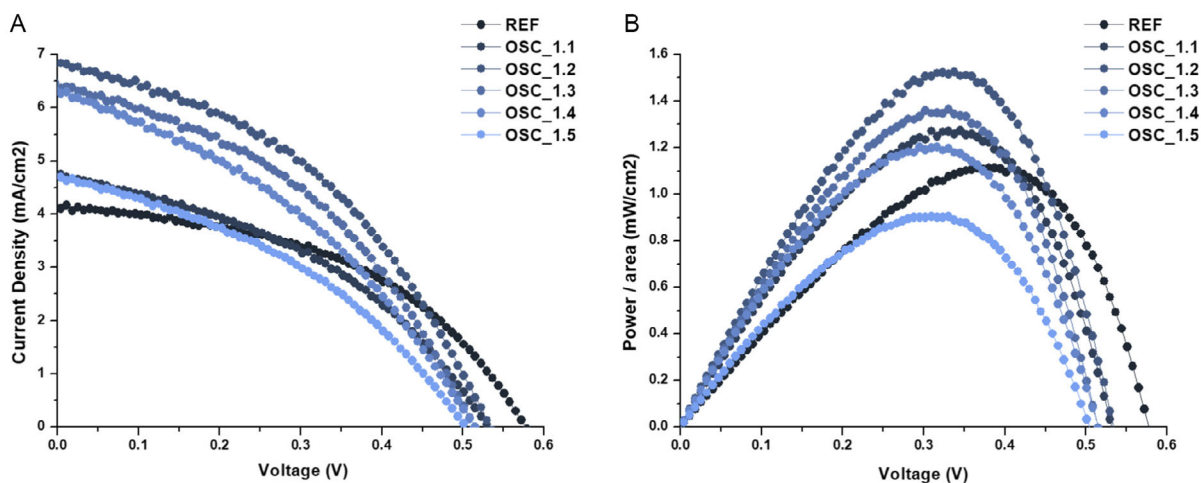


**Figure 3.** A) Current density and B) power/area versus voltage of the reference OSC and the OSCs doped with DMF.

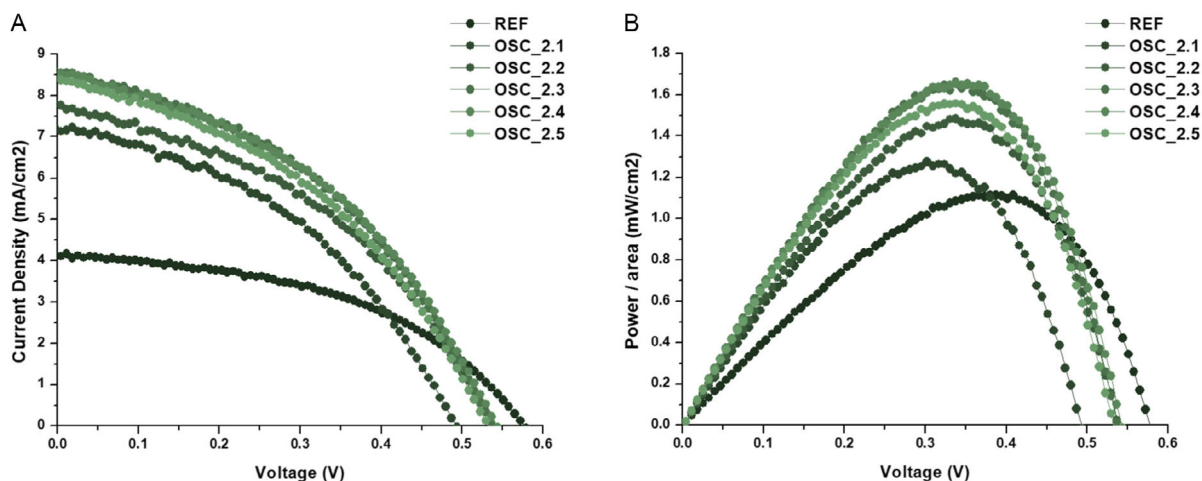


**Figure 4.** A) Current density and B) power/area versus voltage of the reference OSC and the OSCs doped with THF.

**Table 5.** Electrical characteristics of the OSCs doped with THF and OSC without solvent (reference).

OSCs	Reference	OSC_2.1	OSC_2.2	OSC_2.3	OSC_2.4	OSC_2.5
$V_{OC}$ [V]	0.58	0.44	0.46	0.46	0.47	0.46
$J_{SC}$ [ $\text{mA cm}^{-2}$ ]	4.13	7.16	7.77	8.57	8.52	8.38
$P_{MAX}$ [ $\text{mW cm}^{-2}$ ]	1.12	1.28	1.48	1.66	1.65	1.56
FF [%]	47	41	41	42	42	41
PCE [%]	1.11	1.28	1.48	1.66	1.65	1.56

**Table 6.** Electrical characteristics of the OSCs doped with DMSO and OSC without solvent (reference).

OSCs	Reference	OSC_3.1	OSC_3.2	OSC_3.3	OSC_3.4	OSC_3.5
$V_{OC}$ [V]	0.58	0.44	0.44	0.42	0.43	0.44
$J_{SC}$ [ $\text{mA cm}^{-2}$ ]	4.13	7.81	7.91	7.07	6.63	6.20
$P_{MAX}$ [ $\text{mW cm}^{-2}$ ]	1.12	1.21	1.27	1.07	1.01	0.99
FF [%]	47	36	37	36	35	37
PCE [%]	1.11	1.21	1.27	1.07	1.01	0.99

blend.<sup>[29]</sup> In that study, it was also dismissed that the increase in efficiency was due to the thickness of the PEDOT:PSS layer.<sup>[29]</sup> In the manufacturing process of the solar cells, the volumes of the polymer solutions forming the layers of the OSCs are kept constant to maintain device fabrication stability. Similarly, the volume of the PEDOT:PSS solution is 200  $\mu\text{L}$  for all the OSCs; thus, the mass of PEDOT:PSS decreases when the volume of solvent increases. This fact might justify the loss of correlation between the increase in solvent volume and the increase in PCE. Nevertheless, the maximum efficiency is found with approximately the same mass of PEDOT:PSS for all the solvents.

According to the data presented in Table 4–6, two trends could be observed that merit consideration. On one hand, the  $V_{OC}$  could be considered constant regardless of the solvent's presence (with maximum variations of 0.16 V), while on the other hand,

the  $J_{SC}$  exhibits some variability. Furthermore, the variability in current density corresponds with variations in PCE. Observing the study by Khlyabich et al.<sup>[43]</sup> published in 2014, the results of the  $V_{OC}$  in our research could be considered expected. They suggested that modifications in the voltage of OSCs based on BHJs may arise from interactions resulting from the composition of the donor and acceptor materials. In our study, these interactions depend on the polymer blend P3HT:PCBM, which is consistent throughout the experiment and not altered. The trend in current density could be attributed to two factors. The increase in current density may be due to the presence of solvents, which reduces the intermolecular distance between PEDOT and PSS polymers, thereby enhancing carrier mobility.<sup>[29]</sup> However, an excess of solvent in the PEDOT:PSS layer, arising from the device manufacturing process, results in a reduced volume of PEDOT:PSS used in fabrication, potentially explaining the decrease in current density observed in devices with higher solvent volumes.

An association between PCE values and solvent polarity has been identified, as depicted in Figure 6. DMSO exhibits lower efficiency compared to the other solvents (THF with a relative polarity of 0.207, DMF 0.386, and DMSO 0.444, using water as a reference with a relative polarity of 1).<sup>[44]</sup>

The results plotted in Figure 6 appear to contradict the most widely established explanation for justifying the increase in PEDOT:PSS conductivity, which would result in an OSC efficiency enhancement. According to several studies,<sup>[45]</sup> repulsions originating from Coulomb interactions between PEDOT:PSS polymer chains could be reduced by adding a polar solvent such as DMF, THF, and DMSO. This leads to a decrease in the intermolecular distance between the polymers, improving charge transport. Therefore, it was expected that using a solvent with higher relative polarity would further decrease the intermolecular distance, enhancing charge transport in the layer. However, Figure 6 shows the opposite relationship. The solvent with lower relative polarity leads to higher PCE. Even including the results from several experiments performed by our research group along years, we do not obtain a direct trend between polarity of the solvent and PCE increase.

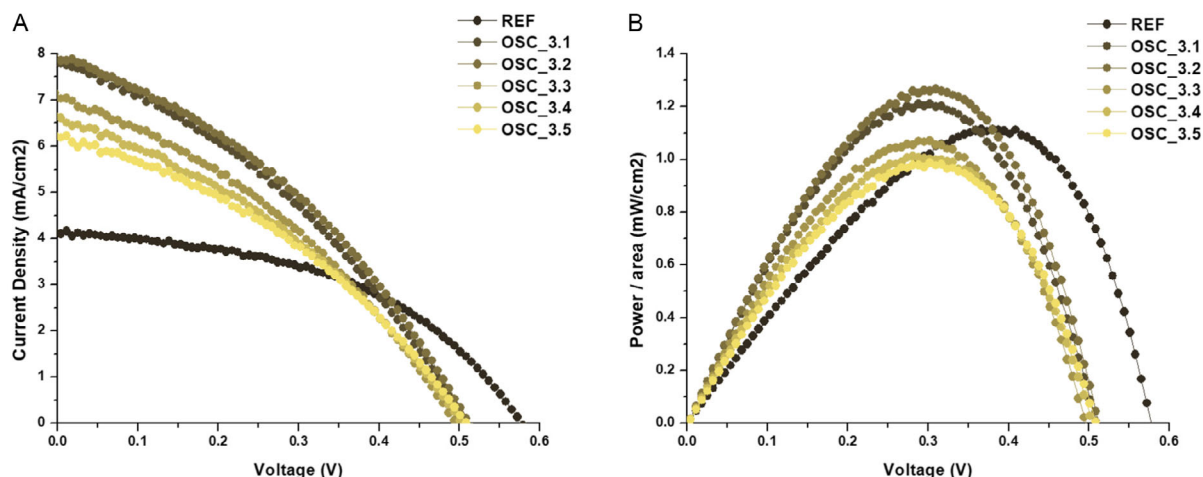


Figure 5. A) Current density and B) power/area versus voltage of the reference OSC and the OSCs doped with DMSO.

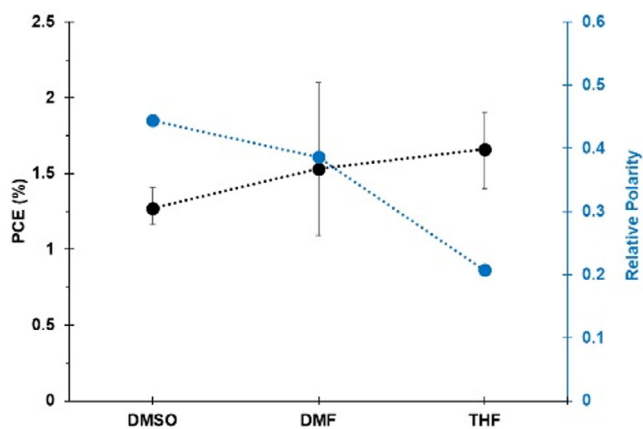


Figure 6. In black, the maximum PCE values of each of the OSCs doped with DMSO, DMF, and THF and the relative polarity (blue) of the solvents. Vertical black line on each PCE value represents the error bar calculated from several sets of experiments equivalent to the one presented in this article.

This apparent contradiction may indicate that polarity is not the sole factor involved in this process. Phase segregation in PEDOT:PSS deposition is another mechanism often related to its conductivity enhancement. In the spin-coating manufacturing technique, various factors such as fluid density or viscosity could modify the layer thickness and consequently affect charge mobility within the layer.<sup>[46]</sup> The different density values of the solvents ( $1.0957 \text{ g cm}^{-3}$  for DMSO,  $0.9445 \text{ g cm}^{-3}$  for DMF, and  $0.8833 \text{ g cm}^{-3}$  for THF<sup>[47]</sup>) and its different viscosity ( $1.984 \text{ mPa s}^{-1}$  for DMSO,  $0.801 \text{ mPa s}^{-1}$  for DMF,<sup>[48]</sup> and  $0.461 \text{ mPa s}^{-1}$  for THF<sup>[49]</sup>) could influence the morphology of the interface between PEDOT:PSS HTL and the active layer altering the electrical characteristics of the device and its PCE value.

### 3.2. Environmental Impact Study

In Section 2.3 of this document, the manufacturing process of the devices studied in this work has been described. The process

is very similar for all devices, except for the composition of the solution that generates the PEDOT:PSS layer. The composition of this solution is described in Table 1 for DMF, Table 2 for THF, and Table 3 for DMSO solvent. Since the process only varies at this step, an environmental impact study will be conducted on the manufacturing of these films. Furthermore, for the completion of this study, the guidelines outlined in the article authored by García-Valverde et al. have been followed.<sup>[50]</sup> The methodology used in the environmental impact analysis was the European center of environmental science of leiden university-impact assessment baseline method, along with the EU25 normalization set, by the SimaPro software. The eleven impact categories associated with this method and normalization set are Abiotic Depletion, Abiotic Depletion (Fossil Fuels) (A. Depletion [F.F.]), Global Warming, Ozone Layer Depletion (Ozone Layer D.), Human Toxicity, Fresh Water Ecotoxicity (Fresh water E.), Marine Aquatic Ecotoxicity (Marine A. E.), Terrestrial Ecotoxicity (Terrestrial E.), Photochemical Oxidation (Photoc. O.), Acidification, and Eutrophication.

The environmental study data indicate that across all impact categories (Table 7 and Figure 7), the utilization of the solvent DMF leads to a reduction in impact. It is noteworthy that the category exhibiting the highest influence of DMF is Abiotic Depletion, decreasing from  $3.47\text{E}-07 \text{ kg Sb eq}$  for solvent-free OSCs to  $9.11\text{E}-08 \text{ kg Sb eq}$  in devices with the highest DMF content in their PEDOT:PSS layer. Conversely, the category where the use of DMF solvent in the manufacturing process has the least influence is Eutrophication. Nonetheless, a significant impact is still observed within this impact category. The solvent-free device produces  $9.75\text{E}-06 \text{ kg PO-eq}$ , whereas it decreases to  $8.68\text{E}-06 \text{ kg PO-eq}$  in the device with the lowest volume of solvent, resulting in a reduction of its impact by over 10%. Furthermore, this reduction is directly proportional to the increase in DMF in the manufacture of OSCs. During the fabrication of DMF-doped solar cells, a substitution of PEDOT:PSS with the solvent takes place, thereby yielding a positive environmental impact for these devices due to PEDOT:PSS being more contaminating than DMF.

Similarly to the use of the solvent DMF, THF reduces contamination across all impact categories when compared to devices

**Table 7.** Environmental impact of different categories in relation to the use of DMF in the OSCs production.

Impact categories	Units	Reference	OSC_1.1	OSC_1.2	OSC_1.3	OSC_1.4	OSC_1.5
Abiotic depletion	kg Sb eq	3.43E−07	1.78E−07	1.43E−07	1.21E−07	1.03E−07	9.11E−08
A. Depletion (F.F.)	MJ	2.39E−01	1.54E−01	1.37E−01	1.25E−01	1.16E−01	1.10E−01
Global Warming	kg CO <sub>2</sub> eq	1.45E−02	8.78E−03	7.59E−03	6.82E−03	6.22E−03	5.79E−03
Ozone layer D.	kg CFC-11 eq	1.40E−09	9.28E−10	8.31E−10	7.67E−10	7.17E−10	6.82E−10
Human toxicity	kg 1.4-DB eq	2.13E−03	1.43E−03	1.28E−03	1.18E−03	1.11E−03	1.06E−03
Fresh water E.	kg 1.4-DB eq	1.49E−03	1.02E−03	9.28E−04	8.64E−04	8.15E−04	7.81E−04
Marine A. E.	kg 1.4-DB eq	6.26E+00	4.14E+00	3.69E+00	3.41E+00	3.18E+00	3.02E+00
Terrestrial E.	kg 1.4-DB eq	7.45E−06	4.55E−06	3.95E−06	3.56E−06	3.25E−06	3.04E−06
Photoc. O.	kg C <sub>2</sub> H <sub>4</sub> eq	2.12E−06	1.50E−06	1.37E−06	1.28E−06	1.22E−06	1.17E−06
Acidification	kg SO <sub>2</sub> eq	4.34E−05	2.73E−05	2.39E−05	2.17E−05	2.00E−05	1.88E−05
Eutrophication	kg PO eq	9.75E−06	8.68E−06	8.45E−06	8.31E−06	8.20E−06	8.12E−06

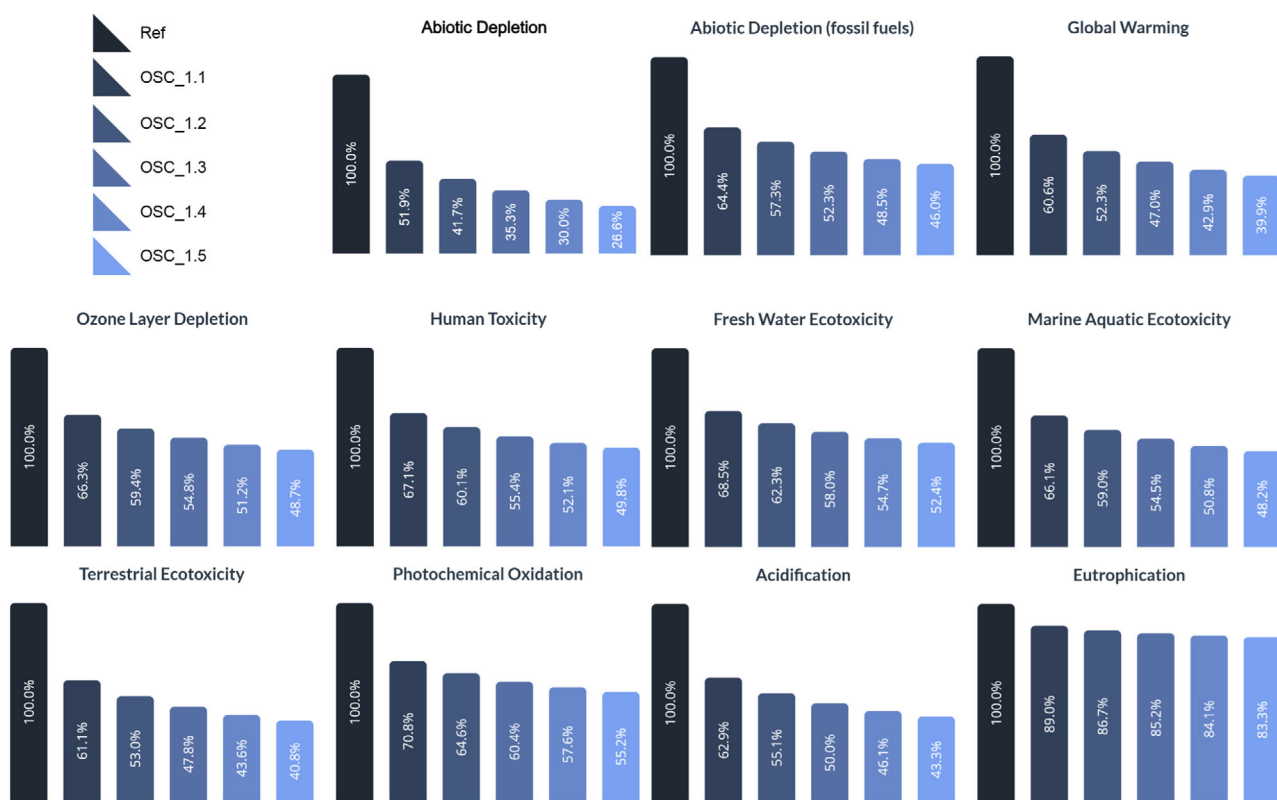


**Figure 7.** Environmental impact of different categories normalized to solar cells without DMF (Reference) in the OSCs production.

without any solvent, see **Table 8** and **Figure 8**. It is noteworthy that the greatest influence of THF occurs in the same category as DMF, Abiotic Depletion. In this category, solvent-free OSCs produce 3.43E−07 kg Sb eq, while the OSC with the highest volume of solvent produces 1.10E−07 kg Sb eq.

As observed in the DMF and THF series, OSCs fabricated using DMSO in the formation of the PEDOT:PSS layer also exhibit a reduction in impact across all categories, with its

influence being greater as more volume of solvent is employed (**Table 9**, **Figure 9**). Furthermore, akin to OSCs using DMF and THF, the impact category most affected was Abiotic Depletion.

In all series, it was observed that the use of solvents in the PEDOT:PSS layer leads to a substantial improvement across all impact categories in environmental impact studies. This improvement may be attributed to the fact that the use of these solvents results in a reduction in the volume of PEDOT:PSS used

**Table 8.** Environmental impact of different categories in relation to the use of THF in the OSCs production.

Impact categories	Units	Reference	OSC_2.1	OSC_2.2	OSC_2.3	OSC_2.4	OSC_2.5
Abiotic depletion	kg Sb eq	3.43E−07	2.39E−07	1.85E−07	1.51E−07	1.28E−07	1.10E−07
A. Depletion (F.F.)	MJ	2.39E−01	1.93E−01	1.69E−01	1.54E−01	1.44E−01	1.36E−01
Global warming	kg CO <sub>2</sub> eq	1.45E−02	1.18E−02	1.03E−02	9.44E−03	8.85E−03	8.39E−03
Ozone layer D.	kg CFC-11 eq	1.40E−09	1.11E−09	9.52E−10	8.56E−10	7.93E−10	7.43E−10
Human toxicity	kg 1.4-DB eq	2.13E−03	2.03E−03	1.97E−03	1.94E−03	1.92E−03	1.90E−03
Fresh water E.	kg 1.4-DB eq	1.49E−03	1.48E−03	1.48E−04	1.47E−04	1.47E−04	1.47E−04
Marine A. E.	kg 1.4-DB eq	6.26E+00	6.05E+00	5.93E+00	5.86E+00	5.82E+00	5.78E+00
Terrestrial E.	kg 1.4-DB eq	7.45E−06	6.61E−06	6.17E−06	5.90E−06	5.72E−06	5.57E−06
Photoc. O.	kg C <sub>2</sub> H <sub>4</sub> eq	2.12E−06	1.98E−06	1.90E−06	1.86E−06	1.83E−06	1.80E−06
Acidification	kg SO <sub>2</sub> eq	4.34E−05	3.77E−05	3.46E−05	3.28E−05	3.15E−05	3.05E−05
Eutrophication	kg PO eq	9.75E−06	9.02E−06	8.65E−06	8.41E−06	8.25E−06	8.13E−06

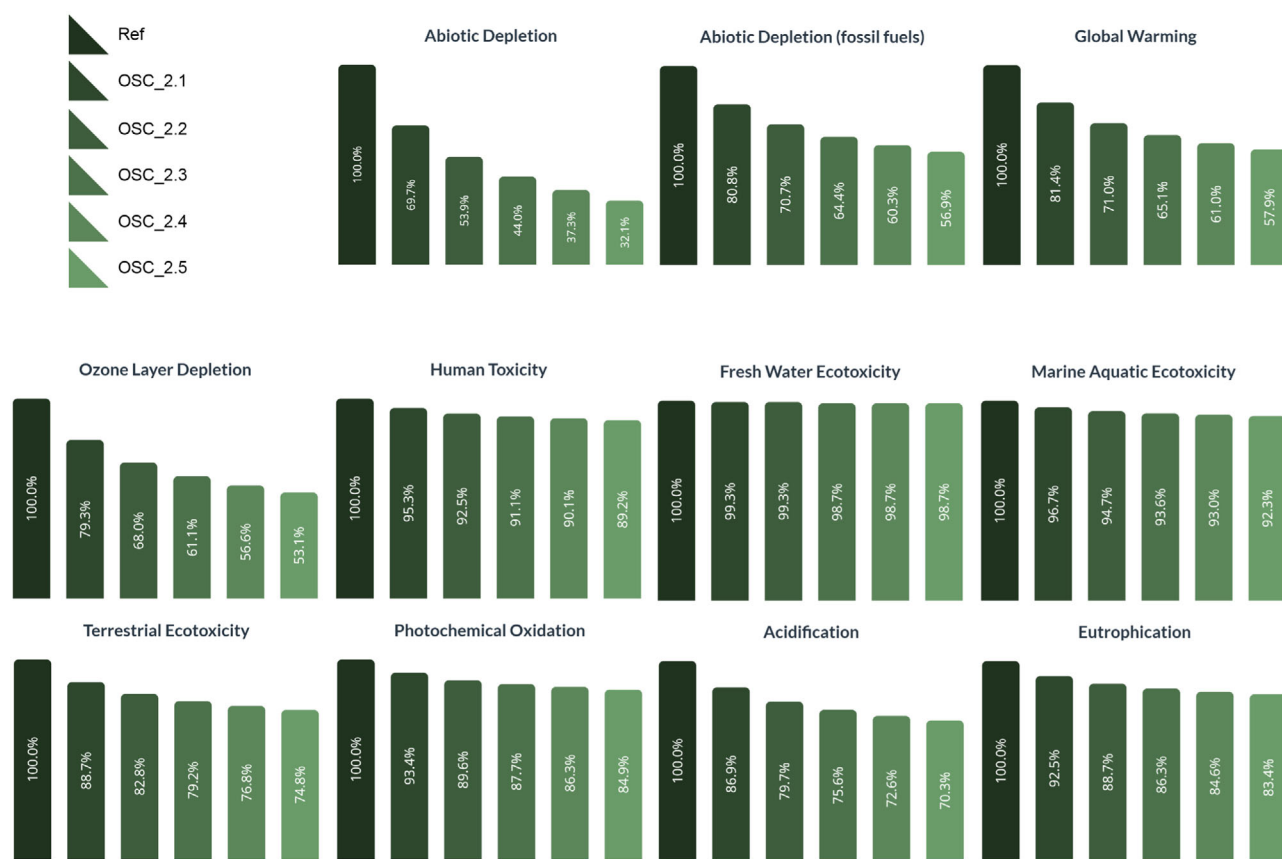


**Figure 8.** Environmental impact of different categories normalized to solar cells without THF (Reference) in the OSCs production.

in the manufacturing process. For this reason, the more solvent was used, the less environmental impact the OSCs produced.

When comparing each of the devices doped with solvents, **Figure 10** (where OSC\_1.5 represents the device doped with DMF at a volume ratio of [1:3.0], OSC\_2.5 represents the device doped with THF at a ratio of [1:2.5], and OSC\_3.5 represents the device doped with DMSO at a ratio of [1:5.0] and impact

categories are defined as follows: IC 01 for Abiotic Depletion, IC 02 for Abiotic Depletion (Fossil Fuels), IC 03 for Global Warming, IC 04 for Ozone Layer Depletion, IC 05 for Human Toxicity, IC 06 for Fresh water Ecotoxicity, IC 07 for Marine Aquatic Ecotoxicity, IC 08 for Terrestrial Ecotoxicity, IC 09 for Photochemical Oxidation, IC 10 for Acidification, and IC 11 for Eutrophication). It can be observed that any



**Table 9.** Environmental impact of different categories in relation to the use of DMSO in the OSCs production.

Impact Categories	Units	Reference	OSC_3.1	OSC_3.2	OSC_3.3	OSC_3.4	OSC_3.5
Abiotic depletion	kg Sb eq	3.43E-07	1.64E-07	1.01E-07	8.12E-08	6.50E-08	5.37E-08
A. Depletion (F.F.)	MJ	2.39E-01	1.34E-01	9.48E-02	8.56E-02	7.61E-02	6.95E-02
Global warming	kg CO <sub>2</sub> eq	1.45E-02	7.52E-03	4.98E-03	4.28E-03	3.65E-03	3.21E-03
Ozone layer D.	kg CFC-11 eq	1.40E-09	7.79E-10	5.46E-10	4.90E-10	4.34E-10	3.95E-10
Human toxicity	kg 1.4-DB eq	2.13E-03	1.19E-03	8.32E-04	7.47E-04	6.62E-04	6.02E-04
Fresh water E.	kg 1.4-DB eq	1.49E-03	8.32E-04	5.84E-04	5.25E-04	4.66E-04	4.24E-04
Marine A. E.	kg 1.4-DB eq	6.26E+00	3.38E+00	2.31E+00	2.03E+00	1.77E+00	1.59E+00
Terrestrial E.	kg 1.4-DB eq	7.45E-06	3.88E-06	2.57E-06	2.21E-06	1.89E-06	1.66E-06
Photoc. O.	kg C <sub>2</sub> H <sub>4</sub> eq	2.12E-06	1.29E-06	9.60E-07	9.01E-07	8.26E-07	7.74E-07
Acidification	kg SO <sub>2</sub> eq	4.34E-05	2.58E-05	1.89E-05	1.75E-05	1.59E-05	1.48E-05
Eutrophication	kg PO eq	9.75E-06	5.28E-06	3.62E-06	3.20E-06	2.79E-06	2.51E-06

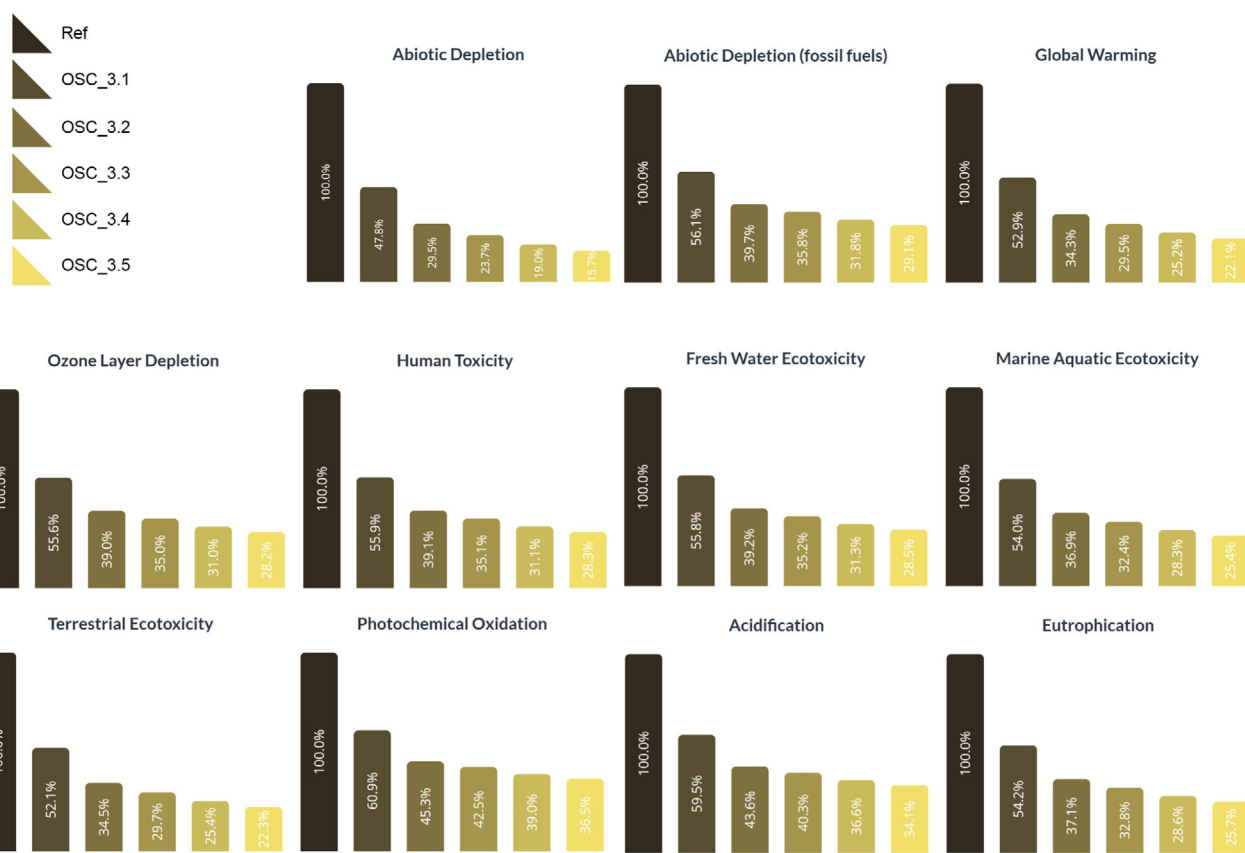


**Figure 9.** Environmental impact of different categories normalized to solar cells without DMSO (Reference) in the OSCs production.

inclusion of solvent yields improved environmental impact data when normalized to the device without solvents.

In Figure 10, the environmental impact assessment of devices exhibiting the greatest decrease in environmental impact within each solvent series has been compared. Among the solvents tested, DMSO yields the most favorable results, followed by DMF and THF. However, device OSC\_3.5

used 167  $\mu\text{L}$  of DMSO solvent in the PEDOT:PSS film, OSC\_1.5 used 150  $\mu\text{L}$  of DMF solvent, and OSC\_2.5 used 143  $\mu\text{L}$  of THF solvent. To rule out that the determining factor for assessing the environmental impact is the amount of solvent used, devices with an equal amount of solvent will be compared to analyze the impact of each solvent on environmental impact.

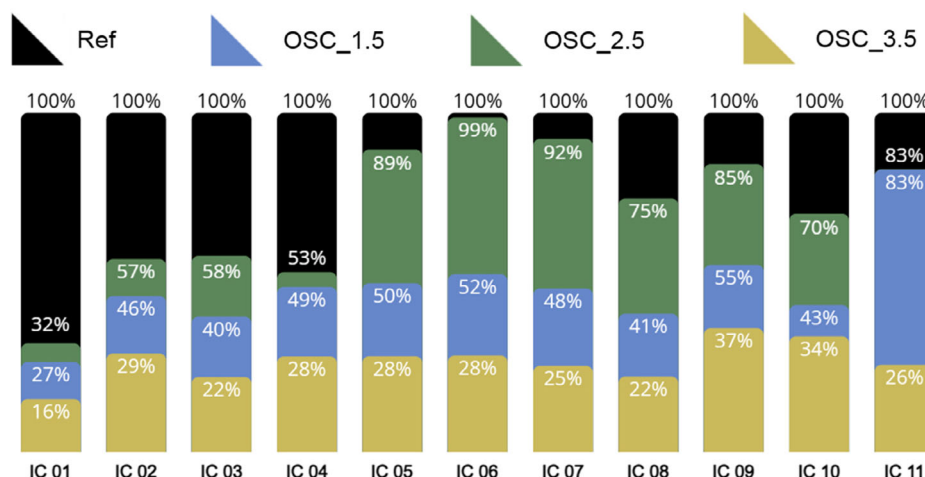


**Figure 10.** Comparison of the devices that have achieved the best results when normalized to the solvent-free OSC.

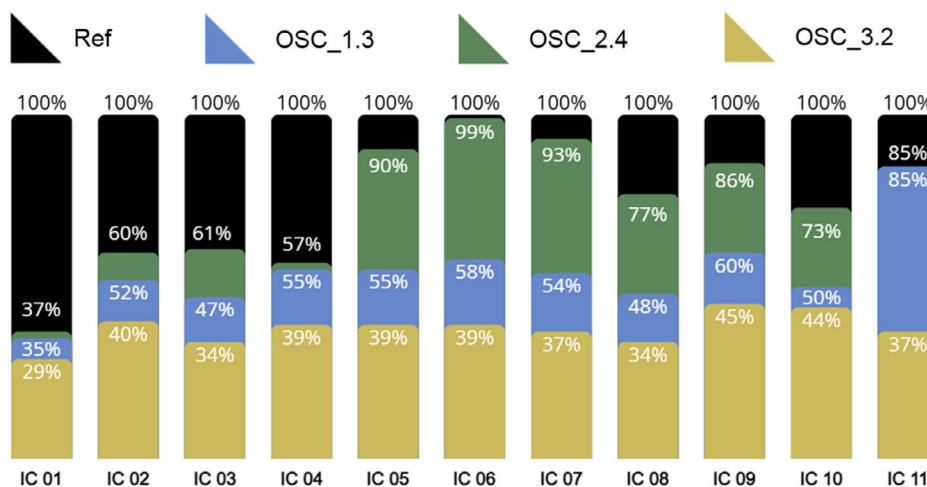


**Figure 11.** Comparison of devices with the same solvent volume when normalized with respect to solvent-free OSC.

The comparison between OSCs where the PEDOT:PSS layer consists of two parts of solvent per volume and one of PEDOT:PSS (OSC\_1.3 for DMF, OSC\_2.4 for THF, and OSC\_3.2 for the solvent DMSO) is shown in **Figure 11**. In this comparative analysis, the influence of each solvent on environmental impacts can be examined in more detail, as the ratio between the volume of PEDOT:PSS and the volume of solvent is the same in all cases. It is observed that the solvent the lowest environmental impact is DMSO, followed by DMF, while THF exhibits the least improvement compared to the reference.

#### 4. Conclusion

In conclusion, the results of the electrical characterization of OSCs doped with different solvents in the PEDOT:PSS layer reveal significant improvements in energy conversion efficiency, particularly when employing polar solvents such as DMF and

THF. These solvents appear to promote a better PEDOT:PSS layer structure, leading to enhance efficiency in electricity generation from sunlight. However, it is important to note that an increase in solvent volume may diminish the efficacy of the PEDOT:PSS layer, highlighting the importance of striking an optimal balance in the layer formulation to maximize overall OSC efficiency.

Regarding environmental impact study, it indicates that the inclusion of solvents in OSC manufacturing can notably decrease environmental impact across various categories, particularly Abiotic Depletion. This suggests that OSCs have the potential to serve as a more sustainable alternative compared to traditional silicon-based solar cell technologies. However, further research is needed to fully assess the life cycle and overall environmental impact of OSCs compared to other solar technologies. In conclusion, these findings support the feasibility and promise of OSCs as a cleaner and more sustainable energy option for the future.

## Conflict of Interest

The authors declare no conflict of interest.

## Data Availability Statement

Data sharing is not applicable to this article as no new data were created or analyzed in this study.

## Keywords

dimethylformamide, dimethyl sulfoxide, environmental impacts, organic solar cells, poly(3-hexylthiophene)-[6,6]-phenyl-C61-butyric acid methyl ester, tetrahydrofuran

Received: July 1, 2024

Revised: July 16, 2024

Published online:

- [1] V. Smil, in *Energy Transitions: Global and National Perspectives*, 2nd ed., Praeger, Santa Barbara, California **2016**.
- [2] B. Hrnčić, A. Pfeifer, F. Jurić, N. Duić, V. Ivanović, I. Vušanović, *Energy* **2021**, 237, 121526.
- [3] D. Gielen, F. Boshell, D. Saygin, M. D. Bazilian, N. Wagner, R. Gorini, *Energy Strategy Rev.* **2019**, 24, 38.
- [4] K. Pytel, M. Melnyk, W. Hudy, F. Kurdziel, A. Kalwar, S. Gumula, in *2020 IEEE XVth Int. Conf. on the Perspective Technologies and Methods in MEMS Design (MEMSTECH)*, Lviv, Ukraine **2020**.
- [5] A. M. Mitrašinović, *Energy* **2021**, 237, 121510.
- [6] K. Blok, A. Afanador, I. van der Hoorn, T. Berg, O. Y. Edelenbosch, D. P. van Vuuren, *Energies* **2020**, 13, 943.
- [7] M. F. Hossain, *Renewable Sustainable Energy Rev.* **2017**, 73, 695.
- [8] R. Blazy, J. Blachut, A. Ciepiela, R. Labuz, R. Papież, *Front. Energy Res.* **2021**, 9, 767418.
- [9] R. Ramanathan, L. S. Ganesh, *Energy Convers. Manage.* **1994**, 35, 661.
- [10] A. Albatayneh, R. Albadaineh, A. Juaidi, R. Abdallah, M. D. G. Montoya, F. Manzano-Agugliaro, *Energy Rep.* **2022**, 8, 4223.
- [11] D. N. Karamov, I. M. Minarchenko, P. V. Ilyushin, K. V. Suslov, S. P. Filippov, *Energy Rep.* **2022**, 8, 1377.
- [12] R. Wolniak, B. Skotnicka-Zasadzień, *Energies* **2022**, 15, 662.
- [13] A. Ghosh, V. K. S. Prasad, *Energy Rev.* **2024**, 190, 114047.
- [14] D. Chemisana, *Renewable Sustainable Energy Rev.* **2011**, 15, 603.
- [15] Y. He, Y. Che, Y. Lyu, Y. Lu, Y. Zhang, *Renewable Energy* **2022**, 187, 1065.
- [16] M. Jaber, *Front. Commun. Networks* **2023**, 4, 1219047.
- [17] N. Baghel, K. Manjunath, A. Kumar, *Comput. Electr. Eng.* **2023**, 110, 108849.
- [18] R. Chandel, S. S. Chandel, D. Prasad, R. P. Dwivedi, *J. Cleaner Prod.* **2024**, 442, 141099.
- [19] K. Dolge, D. Blumberga, *Environ. Clim. Technol.* **2022**, 26, 616.
- [20] A. Hamdan, B. Alareeni, R. Khamis, R. M. Dahlan, *J. Decis. Syst.* **2022**, 33, 195.
- [21] K. Guzik, A. Burkowicz, J. Szlugaj, *Gospod. Surowcami Miner.* **2022**, 38, 31.
- [22] F. Corcelli, M. Ripa, S. Ulgiati, *J. Cleaner Prod.* **2017**, 161, 1129.
- [23] X. Gu, X. Yu, D. Yang, *Sep. Purif. Technol.* **2011**, 77, 33.
- [24] Y. Yu, X. Bai, S. Li, J. Shi, L. Wang, F. Xi, W. Ma, R. Deng, *Curr. Opin. Green Sustainable Chem.* **2023**, 44, 100870.
- [25] S. Bouarab, F. Mokhtari, S. Kaddeche, D. Henry, V. Botton, A. Medelfef, *J. Cryst. Growth* **2020**, 529, 125298.
- [26] K. W. Tsai, G. Madhaiyan, L. H. Lai, Y. T. Hsiao, J. L. Wu, C. Y. Liao, C. H. Hou, J. J. Shyue, Y. M. Chang, *ACS Appl. Mater. Interfaces* **2022**, 14, 38004.
- [27] B. Arredondo, B. Romero, J. M. S. Pena, A. Fernández-Pacheco, E. Alonso, R. Vergaz, C. de Dios, *Sensors* **2013**, 13, 12266.
- [28] D. Valiente, F. Rodríguez-Mas, J. V. Alegre-Requena, D. Dalmau, J. C. Ferrer, arXiv **2024**.
- [29] F. Rodríguez-Mas, S. Fernández de Ávila, J. C. Ferrer, J. L. Alonso, D. Valiente, *Opt. Mater.* **2023**, 145, 114411.
- [30] S. K. Dey, N. B. Manik, S. Bhattacharya, A. N. Basu, *Synth. Met.* **2001**, 118, 19.
- [31] E. Lopez-Fraguas, B. Arredondo, C. Vega-Colado, G. del Pozo, M. Najafi, D. Martin-Martin, Y. Galagan, J. M. Sánchez-Pena, R. Vergaz, B. Romero, *Org. Electron.* **2019**, 73, 292.
- [32] H. M. Schrickx, S. Gyurek, C. Moore, E. Hernandez-Pagan, C. J. Doherty, M. W. Kudenov, T. O'Connor, *Adv. Opt. Mater.* **2024**, 12, 202400005.
- [33] P. Wei, J. H. Oh, G. Dong, Z. Bao, *J. Am. Chem. Soc.* **2009**, 132, 8852.
- [34] N. Sharma, C. M. S. Negi, M. Sharma, A. S. Verma, S. K. Gupta, *Opt. Mater.* **2019**, 95, 109273.
- [35] J. Piris, T. E. Dykstra, A. A. Bakulin, P. H. M. van Loosdrecht, W. Knulst, M. T. Trinh, J. M. Schins, L. D. A. Siebbeles, *J. Phys. Chem. C* **2009**, 113, 14500.
- [36] M. M. de Kok, M. Buechel, S. I. E. Vulto, P. van de Weijer, E. Meulenkamp, S. H. P. M. de Winter, A. J. G. Mank, H. J. M. Vorstenbosch, C. H. L. Weijtens, V. van Elsbergen, *Phys. Status Solidi A* **2004**, 6, 1342.
- [37] S. H. Jeong, S. Ahn, T. W. Lee, *Macromol. Res.* **2019**, 27, 2.
- [38] B. Friedel, P. E. Keivanidis, T. J. K. Brenner, A. Abrusci, C. R. McNeill, R. H. Friend, N. C. Greenham, *Macromolecules* **2009**, 42, 6741.
- [39] K. S. Reddy, B. S. Veeralingam, P. H. Borse, S. Badhulika, *J. Alloys Compd.* **2022**, 919, 165775.
- [40] Y. Xia, J. Ouyang, *J. Mater. Chem.* **2011**, 21, 4927.
- [41] M. M. U. Zaman, M. Imran, A. Saleem, A. H. Kamboh, M. Arshad, N. A. Khan, P. Akhter, *Phys. B: Condens. Matter* **2017**, 522, 57.
- [42] Z. Çaldıran, Ü. Erkem, A. Baltakesmez, M. Biber, *Phys. B: Condens. Matter* **2021**, 607, 412859.
- [43] P. P. Khyabich, A. E. Rudenko, R. A. Street, B. C. Thompson, *ACS Appl. Mater. Interfaces* **2014**, 6, 9913.
- [44] C. Reichardt, T. Welton, in *Solvent Effects in Organic Chemistry*, Wiley, Hoboken, NJ **2010**.
- [45] N. A. Shahrim, Z. Ahmad, A. W. Azman, Y. F. Buys, N. Sarifuddin, *Mater. Adv.* **2021**, 2, 7118.
- [46] N. Sahu, B. Parija, S. Panigrahi, *Indian J. Phys.* **2009**, 83, 493.
- [47] T. M. Aminabhavi, V. B. Patil, *J. Chem. Eng. Data* **1998**, 43, 497.
- [48] J. G. Baragi, M. I. Aralaguppi, T. M. Aminabhavi, M. Y. Kariduraganavar, A. S. Kittur, *J. Chem. Eng. Data* **2005**, 50, 910.
- [49] B. Giner, I. Gascón, A. Villares, P. Cea, C. Lafuente, *J. Chem. Eng. Data* **2006**, 51, 1321.
- [50] R. García-Valverde, J. A. Cherni, A. Urbina, *Prog. Photovoltaics* **2017**, 18, 535.